Speedup of Doping Fronts in Organic Semiconductors through Plasma Instability

V. Bychkov, P. Matyba, V. Akkerman, M. Modestov, D. Valiev, G. Brodin, C. K. Law, M. Marklund, and L. Edman

Phys. Rev. Lett. **107**, 016103 — Published 30 June 2011

DOI: 10.1103/PhysRevLett.107.016103

Speedup of doping fronts in organic semiconductors through plasma instability

V. Bychkov[1], P. Matyba[1], V. Akkerman[2], M. Modestov[1],
D. Valiev[1], G. Brodin[1], C. K. Law[2,3], M. Marklund[1], and L. Edman[1]
[1] *Department of Physics, Umeå University, SE-90187 Umeå, Sweden*
[2] *Department of Mechanical and Aerospace Engineering, Princeton University, Princeton, NJ 08544-5263, USA*
[3] *Center for Combustion Energy, Tsinghua University, Beijing 100084, China*

The dynamics of doping transformation fronts in organic semiconductor plasma is studied for application in light-emitting electrochemical cells. We show that new fundamental effects of the plasma dynamics can significantly improve the device performance. We obtain an electrodynamic instability, which distorts the doping fronts and increases the transformation rate considerably. We explain the physical mechanism of the instability, develop theory, provide experimental evidence, perform numerical simulations and demonstrate how the instability strength may be amplified technologically. The electrodynamic plasma instability obtained also shows interesting similarity to the hydrodynamic Darrieus–Landau instability in combustion, laser ablation, and astrophysics.

Organic semiconductors (OSCs) offer unique and attractive properties, which are expected to revolutionize everyday electronics and stimulate the emergence of "organic electronics" with a large number of novel applications [1–3]. Experimental and technical activities on the subject are extremely high [4–7]; although further development of organic electronics requires much better fundamental understanding of the complex OSC plasma dynamics: electrons, holes, positive and negative ions immersed in an electrolyte. Though much theoretical work has been performed on plasmas in conventional inorganic semiconductors, e.g. [8, 9], for OSCs such understanding is far from being adequate. The key phenomenon is the doping transformation accompanied by significant changes in important material properties: conductivity, color, volume, etc. [2]. Specifically, during n-type (p-type) doping, electrons (holes) are injected into the OSC from the cathode (anode) and compensated by redistribution of cations (anions) in the electrolyte. When the OSC plasma is populated by light charges, its conductivity increases by two-to-three orders of magnitude as compared to the original ion conductivity. In light-emitting electrochemical cells (LECs), doping transformation occurs as propagating fronts [4–7], which may be compared to flames, laser deflagration and fronts of phase transitions [10–14]. When the doping fronts meet, electron-hole annihilation in the p-n junction produces visible light [7, 15–19]. Since the doping rate is controlled by the low mobility of the heavy ions, then the LECs are slow to turn; speedup of the doping process is thus vitally important for organic electronics devices.

Here we obtain the electrodynamic plasma instability of the doping fronts, which leads to much faster kinetics of the process. This instability will be experimentally explored, for the first time. Using previous results for planar doping fronts [20], we shall develop the theory of the instability and perform numerical modeling, which shows good agreement with the experimental results. We shall demonstrate that the strong instability, facilitated by a corrugated pattern in the electrode surfaces, increases the doping rate by a factor of 2 and consequently improves the device kinetics.

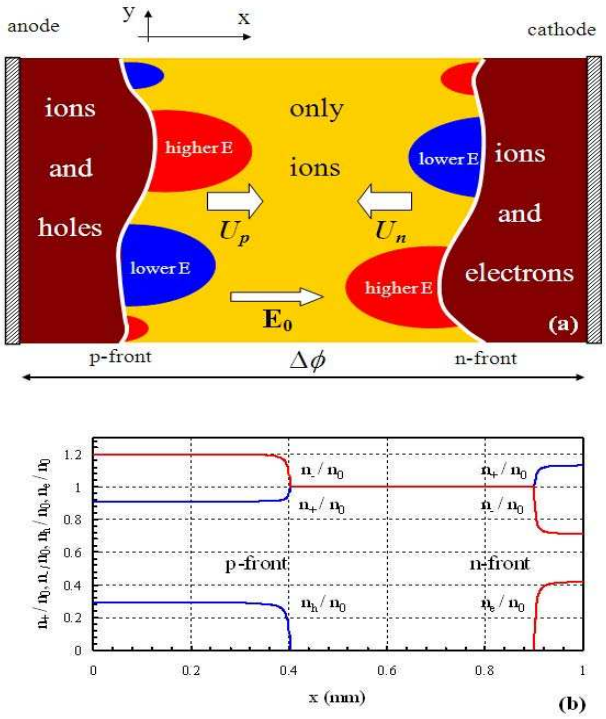

FIG. 1: (a) Schematic of the p- and n-doping fronts in an organic semiconductor film; (b) internal structure of the planar fronts at 90 s.

The configuration of two doping fronts counter-propagating towards each other in an LEC device is schematically illustrated in Fig. 1 (a). Figure 1 (b) shows the internal structure of two such planar fronts, as calculated using the method of [20]. The doping fronts, however, can never be ideally planar because the unavoidable small perturbations grow with time and distort their shape. The physics behind this new instability is

related to the phenomenon of St. Elmo's fire, which visualizes strong increase in the electric field at sharp convex conducting surfaces by numerous discharges in the surrounding air [21]. In the present configuration, any leading perturbation hump at a doping front causes local increase in the electric field in the undoped region. Since the front velocity is proportional to the electric field, see Eq. (1) below, this stronger electric field will force the front to propagate faster locally, thus producing a positive feedback and an unstable growth of the hump.

To study the instability growth, we employ the p/n-doping front velocity derived according to the mobility-diffusion model of the OSC plasma [20],

$$\mathbf{U}_{p,n} = \pm \frac{n_0}{n_{h,e}} (\mu_+ + \mu_-) \mathbf{E}_0, \qquad (1)$$

where $\mathbf{E}_0 = -\nabla\phi_0$ is the electric field just ahead of the front, n_0 the initial ion concentration, $n_{h,e}$ the final concentration of the holes/electrons behind the front, and μ_+ and μ_- the mobilities of the positive/negative ions. The "$\pm$" signs in Eq. (1) indicate that the p-type (+) and n-type (−) doping fronts propagate in opposite directions. We consider a perturbation Fourier mode $\tilde{X}(t)\exp(iky)$ of a p-doping front $x = X_p(y,t)$ in Fig. 1 (a), which also induces perturbations of the electric field in the undoped region. The doped region may be treated as equipotential due to its high conductivity. The front thickness may be characterized by a length scale L_p, of about 10^{-4}–10^{-3}mm, determined by ionic diffusion [20]. Since the characteristic size of the experimentally observed front perturbations (approximately 0.2mm) is much larger than L_p, then we may treat the front as infinitesimally thin. Most of the time the doping fronts are sufficiently far away from each other, $k(X_n - X_p) \gg 1$, such that the instability of one front is not affected by the other. The linearized form of Eq. (1),

$$\partial_t \tilde{X} = -\frac{n_0}{n_h}(\mu_+ + \mu_-)\partial_x \tilde{\phi}, \quad ikU_p\tilde{X} = \frac{n_0}{n_h}(\mu_+ + \mu_-)\partial_y\tilde{\phi}, \qquad (2)$$

together with the solution to the Laplace equation for the electric potential in the udoped region, $\tilde{\phi} \propto \exp(iky - |k|x)$, yields the equation $\partial_t\tilde{X} = U_p|k|\tilde{X}$ describing the perturbation growth with time. Thus, we obtain an instability for the p-type doping front, where the initially small perturbations grow exponentially as $\tilde{X} \propto \exp(\sigma t)$, with the growth rate $\sigma = U_p|k|$. The same result holds for the n-type doping by replacing U_p with U_n. The resulting dispersion relation $\sigma \propto |k|$ is mathematically similar to the Darrieus-Landau (DL) instability encountered in combustion, astrophysics and laser fusion [10–13]. The role of the electric field in the new instability can also be compared to that of the gas velocity field in flames.

To observe the instability experimentally, we utilize an open planar LEC device, comprising an {MEH-PPV + PEO + KCF_3SO_3} active material positioned between two Au electrodes as described in [20]. Two counter-propagating doping fronts can be distinguished in Fig. 2 (a, b); the dark regions with quenched fluorescence correspond to the doped MEH-PPV; the electrodes are indicated with white dashed lines. When the fronts meet and form a p-n junction, recombination of the holes and electrons can lead to light emission shown in Fig. 2 (c). Figures 2 (a, b) then clearly demonstrate that both doping fronts are unstable with respect to small perturbations, though with different outcomes in the nonlinear stage. The instability of the p-front produces smooth humps with a relatively large scale, about $(0.1 - 0.3)$ mm, while the n-front appears as a combination of thin elongated "fingers". We focus on the p-front dynamics, since p-doping dominates for this choice of OSC sweeping more than 75% of the active material [22].

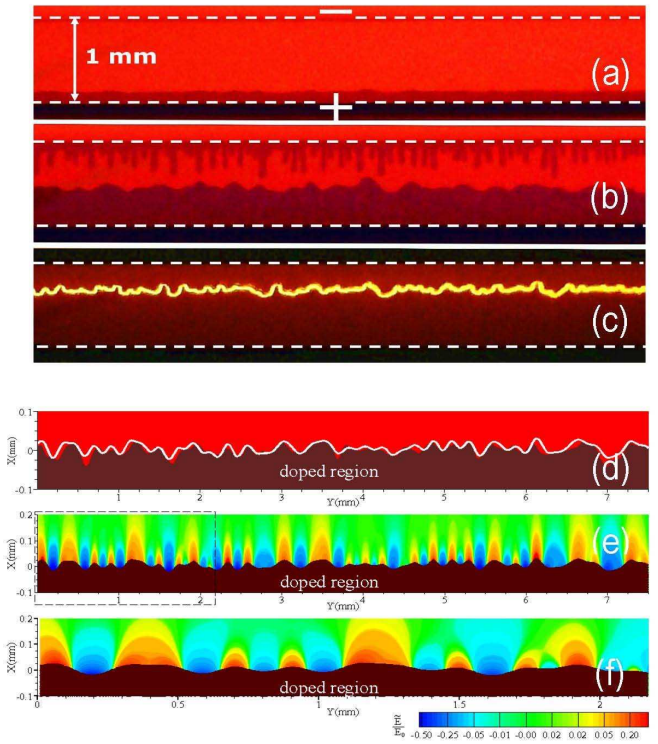

FIG. 2: Experimental photos of the doping fronts demonstrate development of the instability: (a) at the initial stage, $t = 46$ s; (b) at the developed stage, $t = 80$ s; (c) the dynamic p-n junction, $t > 170$ s. The bright line in photo (c), taken in a dark room, is the light-emitting p-n junction, while the remaining part of the sample appears dark. Plot (d) compares the p-front shapes obtained in the simulations (white curve) and experiments (shading) at 70 s. Plots (e), (f) show relative increase in the electric field in the undoped region obtained numerically for: (e) the whole front squeezed along Y-axis; (f) the selected part with equal scales.

A smooth p-doping front allows reducing the full model

to a single nonlinear equation

$$U_p^{-1}\partial_t\tilde{X} = \hat{J}\tilde{X} + (\partial_y\tilde{X})^2 + U_p^{-1}\hat{H}\left[\partial_t\tilde{X}\ \partial_y\tilde{X}\right] + \frac{\lambda_p}{2\pi}\partial_{yy}^2\tilde{X}, \quad (3)$$

where the DL operator $\hat{J}$ and the Hilbert operator $\hat{H}$ imply products by $|k|$ and $|k|/ik$ in Fourier space, respectively. When deriving Eq. (3), we accounted for the nonlinear terms in describing the shape of a distorted front in Eq. (1); a detailed derivation will be presented elsewhere. The last linear term in Eq. (3) describes the stabilization of the instability at short wavelengths below the cut-off $\lambda_p \propto L_p$, which is related to the small front thickness and, therefore, was not accounted in Eq. (2). Though negligible at the experimentally observed length scales, this term avoids the ultraviolet divergence of the numerical solution. Equation (3) has been solved numerically with initial conditions extracted from the experimental data at $t = 10$ s. The numerical modeling reproduces well the characteristic shape of the p-front at later instants, e.g. at $t = 70$ s, see Fig. 2 (d). Figures 2 (e) and (f) show the computed electric field ahead of the corrugated p-type front. The observed increase in the electric field at the humps of the front demonstrates the instability mechanism, as explained earlier. The analytical, experimental, and numerical results for the doping front positions are presented in Fig. 3. The analytical result (solid lines) shows two planar fronts accelerating towards each other. The acceleration occurs because a constant potential difference is effectively applied over the continuously decreasing distance between the doping fronts [23, 24], and because the front velocities are controlled by the potential gradient, Eq. (1). The analytical result relies on our experimental data for ion concentrations and mobilities [20], with the average hole concentration $n_h = 8.6 \cdot 10^{25} m^{-3}$. The p- and n-front velocities diverge as the fronts meet; the front propagation comes to a complete halt at the p-n junction. In the 1D analytical model, the junction is formed simultaneously all over the fronts. In the experiments, the instability makes the fronts curved and the leading parts of the fronts meet in a shorter time, while the slower parts are still propagating.

The experiments reveal a noticeably faster propagation of the cellular doping fronts as compared to the analytical result for planar fronts. In Fig. 3, open diamonds show the mean positions of the experimental non-planar doping fronts, where the "uncertainty" bars indicate the difference between the fastest and the slowest parts of the front brush. The difference can be attributed to the developing instability and the associated wrinkled front, which is not accounted in the analytical description of the planar fronts. The analytical prediction of the positions of the planar fronts correlates well with the slowest points of the experimentally observed fronts, while the leading points in the experiments move approximately 1.4 times faster. In contrast, the numerical modeling of

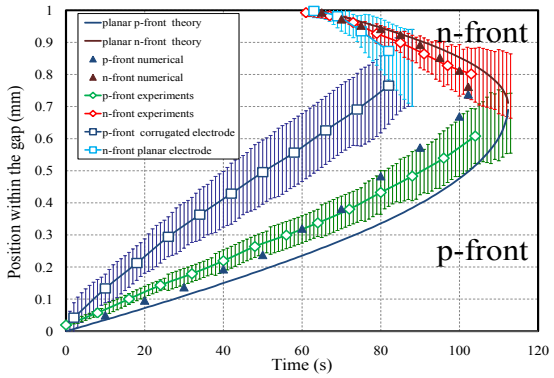

FIG. 3: Mean front position for p- and n-fronts versus time obtained experimentally; predicted theoretically for the planar fronts; and calculated numerically for the wrinkled fronts (see the legend). The error bars of the experimental data indicate the difference in the positions of the fastest and slowest parts of the corrugated front brush.

Eq. (3) does account for the instability and shows good agreement with the experiments. To describe acceleration of the cellular doping fronts towards each other we applied Eq. (3) to both p- and n-fronts. Though Eq. (3) was derived rigorously for the p-front, it describes the average position of the n-front reasonably well within the time interval of the experiments. Reproducing the shape of the n-front and the final light-emitting line in the p-n junction requires further development of the model. We believe that the dynamics of the n-front is affected by electrochemical side-reactions [22] and by small-scale instabilities interacting with that obtained herein.

The present results therefore verify that front instability increases the doping rate. However, the instability theory also indicates that the time and space available for the perturbation growth in the employed LEC devices are not sufficient to achieve a strongly curved front. Specifically, the theory suggests that the instability may increase the velocity of the curved front by a factor of 2 and more as compared to a planar front, which is not observed in the experimental results of Fig. 3 discussed above. Such a strong increase in the front velocity occurs due to the strongly curved humps developed at the front (see the insert of Fig. 4). Therefore, to achieve a strongly curved front and a faster turn-on, we have triggered the instability growth by modifying the initial conditions so that the slowest initial stage of hump growth from natural "white-noise" perturbations is eliminated. Figure 4 presents results from an experiment with a corrugated pattern introduced as the surface of the anode (see the dotted line); the corrugation size was comparable to the humps observed in Fig. 2. The corrugations, though negligible as compared to the total

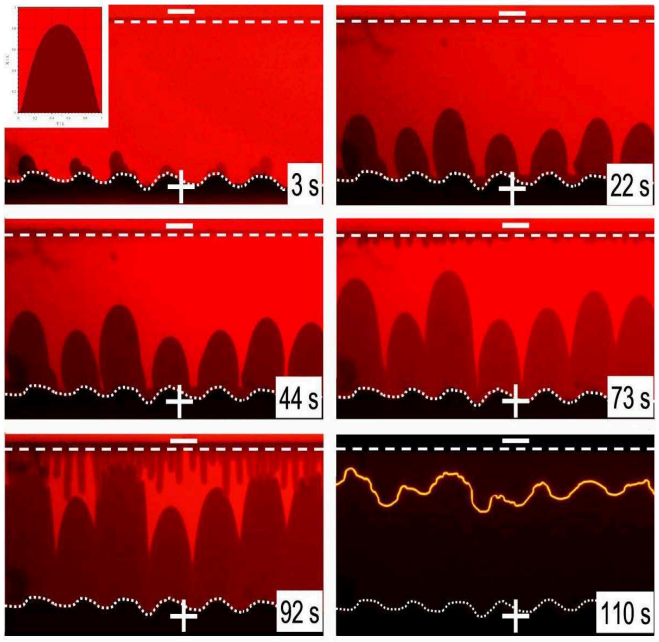

FIG. 4: Experimental photographs showing the time evolution of the p-type doping front in an LEC device with the initial corrugations of the anode. The corresponding time instances are indicated on the photographs. The insert shows a characteristic shape of a strongly curved hump obtained in the theory.

(1 mm) width of the active material, were anticipated to give rise to the desired initial perturbations of the p-type front. Confirming our anticipation, we observed strongly curved and rapidly growing humps at the p-type front, see Fig. 4. The position of the humps in this experiment is also included in Fig. 3, which shows that, in devices with a corrugated electrode surface, the doping rate may increase significantly; by a factor of 2 in the present case. Remarkably, the relative speed-up of the doping fronts is considerably stronger and the humps are much more pronounced than one finds for the DL instability in flames and laser deflagration [11–13]. We have also performed experiments with corrugations included in both the cathode and anode, and, as expected, we observed intensified front dynamics and much faster turn on. By introducing corrugations on the cathode we also find that the initial delay in the development of the n-type front was reduced.

To summarize, we have demonstrated theoretically and experimentally that electrochemical doping fronts in OSC plasmas are unstable. The instability distorts the fronts and increases the doping rate considerably. This understanding of new fundamental effects in OSCs plasmas was utilized in the design of LECs with the turn-on times reduced by a factor of 2 for an OSC film; in the case of a bulk (3D) geometry further increase of the doping rate, by a factor of 3, is expected.

The authors are grateful to Kempestiftelserna, Carl Tryggers Stiftelse, and the Swedish Research Council (VR) for financial support. L.E. is a “Royal Swedish Academy of Sciences Research Fellow” supported by a grant from the Knut and Alice Wallenberg Foundation.

[1] Pei Q. B., Yu G., Zhang C., Yang Y., Heeger A. J., Science **269**, 5227, 1086 (1995).
[2] Leger M. J., Adv. Mater. **20**, 837841 (2008).
[3] Arkhipov V. I., Emalianova E. V., Heremans P., Bassler H., Phys. Rev. B **71**, 235202 (2005).
[4] Gao J., Dane J., Applied Physics Letters **84**, 2778 (2004).
[5] Matyba P., Andersson M.R., Edman L., Organic Electronics, **9** 699 (2008).
[6] Lin, F. D., Walker, E. M., Lonergan, M. C., J. Phys. Chem. Lett. **1** 720 (2010).
[7] Matyba P., Maturova K., Kemerink M., Robinson N.D., Edman L., Nature Mat. **8**, 672 (2009).
[8] F. Haas, G. Manfredi, P. K. Shukla, and P.-A. Hervieux, Phys. Rev. B **80** 073301 (2009).
[9] O. Morandi, P.-A. Hervieux, and G. Manfredi, Phys. Rev. B **81** 155309 (2010).
[10] Zeldovich, Ya.B., Barenblatt, G.I., Librovich, V.B., Makhviladze, G.M., Mathematical Theory of Combustion and Explosions (Consultants Bureau, NY, 1985).
[11] Clanet C., Searby G., Phys. Rev. Lett. **80**, 3867 (1998).
[12] Bychkov V., Liberman M., Dynamics and stability of premixed flames, Phys. Reports **325**, 115 (2000).
[13] Modestov M., Bychkov V., Valiev D., Marklund M., Phys. Rev. E **80**, 046403 (2009).
[14] Inomoto O., Kai S., Malomed B., Phys. Rev. Lett. **85**, 310 (2000).
[15] Rodovsky D. B., Reid O. G., Pingree L. S. C., and Ginger D. S., ACS Nano **4** 2673 (2010).
[16] Slinker J. D., *et al*, Nature Mat. **6** 894 (2007).
[17] Costa, Rubn D., Fernndez, G., Snchez, L., Martn, N., Ort, E., Bolink, Henk J., Chem. Eur. J. **16** 9844 (2010).
[18] Latini, G., Winroth, G., Brovelli, S., McDonnell, S. O., Anderson, H. L., Mativetsky, J. M., Samori, P., Cacialli, F., J. Appl. Phys. **107** 124509 (2010).
[19] Inganas, O., Chem. Soc. Rev. **39**, 2633 (2010).
[20] Modestov M., Bychkov V., Brodin G., Valiev D., Marklund M., Matyba P., Edman L., Phys. Rev. B **81**, 081203(R) (2010).
[21] Landau, L.D., Lifshitz, E.M., Electrodynamics of Continuous Media (Elsevier, Oxford, 2000).
[22] Fang J., Matyba P., Robinson N.D., and Edman L., Journal of the American Chemical Society **130**, 4562 (2008).
[23] Robinson N.D., Shin J.H., Berggren M., and Edman L., Phys. Rev. B **74**, 155210 (2006).
[24] Smela, E., MRS Bulletin **33** 197 (2008).